Journal of Zhejiang University-SCIENCE C (Computers & Electronics)
ISSN 1869-1951 (Print); ISSN 1869-196X (Online)
www.zju.edu.cn/jzus; www.springerlink.com
E-mail: jzus@zju.edu.cn

Novel serpentine structure design method considering confidence level and estimation precision*

Li-sheng CHEN, Xiao-hua LUO†‡, Jiao-jiao ZHU, Fan-chao JIE, Xiao-lang YAN

(*Institute of VLSI Design, Zhejiang University, Hangzhou 310027, China*)

†E-mail: luoxh@vlsi.zju.edu.cn

Received Oct. 17, 2012; Revision accepted Jan. 23, 2013; Crosschecked Feb. 25, 2013

Abstract: Due to the importance of metal layers in the product yield, serpentine test structures are usually fabricated on test chips to extract parameters for yield prediction. In this paper, the confidence level and estimation precision of the average defect density on metal layers are investigated to minimize the randomness of experimental results and make the measured parameters more convincing. On the basis of the Poisson yield model, the method to determine the total area of all serpentine test structures is obtained using the law of large numbers and the Lindeberg-Levy theorem. Furthermore, the method to determine an adequate area of each serpentine test structure is proposed under a specific requirement of confidence level and estimation precision. The results of Monte Carlo simulation show that the proposed method is consistent with theoretical analyses. It is also revealed by wafer experimental results that the method of designing serpentine test structure proposed in this paper has better performance.

Key words: Poisson yield model, Serpentine test structure, Critical area, Average defect density, Confidence level, Estimation precision

doi:10.1631/jzus.C1200297 **Document code:** A **CLC number:** TN4

1 Introduction

As technology nodes become smaller and chips become more complicated, the manufacturing of integrated circuits (ICs) needs more and more conductive backend layers to connect all circuit cells. Defects on metal layers are easier to result in malfunction of the entire chip than before. Fortunately, accurate yield prediction enables the manufacturer to control the quality of process steps and to make changes in the design before volume production, so risks can be reduced significantly.

The accuracy of yield prediction on metal layers mainly depends on the ability to precisely characterize the defects. Defect densities and defect size distributions are the most important defect parameters. To extract these defect parameters, specially designed test structures are usually used. For metal layers, comb/serpentine test structures are frequently fabricated on test chips to investigate issues about metal defects. Stapper (1973) obtained data with serpentine test structures, named ‘open circuit defect monitors’, which were used to determine defect densities of metal layers. Then comb/serpentine structures were introduced to evaluate defects occurring within the same layer (Sayah and Buehler, 1988; Michalka *et al.*, 1990). Afterwards, serpentine structures were parameterized as a part of test structures libraries to rapidly generate customized test chips for low-power/low-voltage complementary metal-oxide semiconductor (CMOS) processes (Kumar *et al.*, 1997). Subsequently, serpentine test structures were stacked over two metal layers to characterize the impact of the chemical mechanical polishing (CMP) process on multi-level interconnect performance (Fayolle *et al.*, 2000). In recent years, serpentine test structures, sometimes called ‘snake structures’ or ‘meander

‡ Corresponding author

* Project (No. 2009ZX02023-004-1) supported by the National Science and Technology Major Project, China

© Zhejiang University and Springer-Verlag Berlin Heidelberg 2013

structure', were frequently used to investigate various issues about metal layers and yields (Teh *et al.*, 2005; Hess *et al.*, 2006; 2010; Lin *et al.*, 2006; Karthikeyan *et al.*, 2010; Chen *et al.*, 2011; Tamaki *et al.*, 2011; Jeong *et al.*, 2012). All work done by prior researchers used serpentine structures to test defect densities of metal layers or to control back end of line (BEOL) fabrication processes. However, few investigations have been done on the reasons why they chose those certain areas of serpentine structures. The statistical theoretical bases of their choices for sample areas were not explained. To prevent the results from subjecting to stochastic noise, further statistical analyses are necessary.

Intuitively, a larger total area of serpentine structures will result in better yield precision; however, it will occupy more wafer area to fabricate them. On the other hand, a too small total area of serpentine test structures is inappropriate because the statistical randomness of yield results will become very significant. Besides the total area, it is necessary to investigate the area of each serpentine structure. If a serpentine structure occupies an overly large area, the number of serpentine structures without defects will be very small, which will decrease the precision of the tested yield of metal layers. Conversely, the small area of a serpentine structure will prevent the phenomenon of containing multiple metal defects in a serpentine structure, and thus will result in a more precise yield testing result, but more costs will be required.

The design of an area-optimized serpentine structure considering confidence level and estimation precision is proposed in this paper. The mechanisms of metal faults are presented in Section 2, and yield models for metal layers are reviewed for the convenience of subsequent analyses. Section 3 describes the way to determine the appropriate total area of serpentine test structures and the appropriate area of each serpentine structure. The statistical bases to determine the area of serpentine structures are analyzed theoretically. In Section 4, good accordance is shown between simulation results and theoretical analyses. In addition, the performance of this design method is validated by wafer experiments and hypothesis tests in Section 5. The conclusions are described in Section 6.

2 Metal failure mechanisms and yield model for metal layers

When a new processing step is applied or a new technology node is introduced, new failure mechanisms of metal interconnections arise (Lin *et al.*, 2002; Roesch and Hamada, 2004; Wahab *et al.*, 2006; Arumi *et al.*, 2008; Hsu *et al.*, 2009). Generally, defects on metal layers are classified into two types: missing material defects and extra material defects (Khare *et al.*, 1994). Two typical defects of these types obtained from our test chips are shown in Fig. 1. Extra material defects may originate from dust on the wafer surface, particles in chemicals, and dirt on photolithographic patterns. Generally, extra material defects in conducting layers may cause short circuit failures, while extra material defects in insulating layers may cause open circuit failures. Missing material defects may come from dust on the wafer surface, missing material in photolithographic patterns, and over-etching on local metal lines. In conducting layers, if the size of a missing material defect is larger than the width of the metal line, an open circuit failure may occur. Similarly, in insulating layers, if the size of a missing material defect is larger than the space between two metal lines, a short circuit failure probably will arise. Since both two types of defects may cause open circuit and short circuit failures, to facilitate analysis, only open circuit failures of metal layers are focused in this paper.

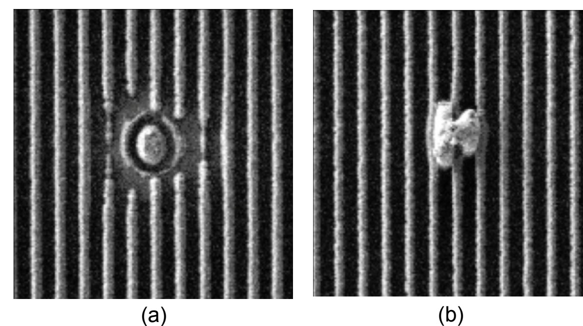

Fig. 1 Missing material defect (a) and extra material defect (b) on metal lines

Note that not every metal defect has an influence on the connectivity of a circuit. The size and location of each defect determine whether a defect will cause a

fault in the implemented electrical network. Yield models are used to associate metal defects with metal failures. Wallmark (1960)'s yield model is the earliest used yield model. With the development of semiconductor technology, many other yield models have been proposed for better yield prediction. The Poisson yield model is one of the yield models frequently used.

The serpentine structure can also be depicted by the Poisson yield model. The average defect density $\bar{D}$ can be estimated by (Stapper, 1983)

$$\bar{D} = -\frac{\ln Y_{\mathrm{s}}}{\bar{A}_{\mathrm{s}}} = -\frac{\ln\left(H_{\mathrm{s}}/N_{\mathrm{s}}\right)}{\bar{A}_{\mathrm{s}}}, \tag{1}$$

where Y_{s} is the yield of serpentine test structures, $\bar{A}_{\mathrm{s}}$ is the average critical area of a serpentine test structure, N_{s} is the number of serpentine test structures used in testing, and H_{s} is the number of serpentine test structures having no fault. The average critical area $\bar{A}_{\mathrm{s}}$ can be obtained by integrating the critical area function with the probability distribution function over all defect sizes (Stapper, 1983). For a serpentine test structure, the average critical area can be acquired by the way to calculate the average critical area of a large number of parallel conductive lines on a chip (Stapper, 1984):

$$\bar{A}_{\mathrm{s}} = \frac{LHx_0^2}{2w(2w+s)}, \tag{2}$$

where w is the line width, s is the space between metal lines, L is the line length, H is the width of each test chip, and x_0 is the defect size where the probability distribution function reaches the peak.

Let θ be the probability of failure, which can be obtained by dividing the average critical area $\bar{A}_{\mathrm{s}}$ by the chip area A_{sc}, so the average critical area can be expressed as (Stapper, 1983)

$$\bar{A}_{\mathrm{s}} = \theta A_{\mathrm{sc}}. \tag{3}$$

Using Eqs. (1)–(3), the requirements for the total area of serpentine test structures and the area of each serpentine structure can be derived in Section 3.

3 Serpentine structure considering confidence level and estimation precision

Serpentine test structures frequently appear in test chips to investigate open defects of metal layers. The total area of serpentine test structures needs to be large enough to guarantee the precision of the measured metal yield. This is because statistical randomness will become very significant with the use of a small area of serpentine structures. On the contrary, the total area of serpentine structures cannot be too large when testing costs and utilization efficiency of the wafer area are taken into account. Then the issue of how large an area is adequate for a certain precision demand is meaningful.

Moreover, the precision of measured metal yield is not only related to the total area of serpentine structures but also related to the area of each serpentine structure. Of course, in theory, a long metal line of test structure can be fabricated containing just one metal line. In this situation, the measured open metal yield approaches the actual yield in a high degree, but no foundry can bear such large testing costs. In reality, a serpentine structure made up of many parallel metal lines is a preferable choice. Though the precision of the measured result is decreased, a tolerable estimation precision can be guaranteed by controlling the area of each serpentine structure. An overly large area of each serpentine structure will lead to most of the test structures containing multiple faults. Consequently, the number of serpentine test structures with no defects will be too small, which will decrease the accuracy of the metal yield.

Therefore, to improve the estimation precision of the measured results and make the yield more convincing, it is important to consider the total area of serpentine test structures and the area of each serpentine structure, which can be further determined by confidence level and estimation precision when designing serpentine test structures.

3.1 Total area of serpentine test structures

As an important structure to characterize open defects on metal layers, serpentine test structures are usually used to extract the parameter of average defect density. Assuming M is the number of open serpentine structures and $\bar{A}_{\mathrm{t}}$ is the total average critical area of all serpentine structures, then M is a random

variable and it obeys the Poisson distribution (Stapper, 1983). To improve the accuracy of the measured average defect density, the requirements for $\bar{A}_t$ can be expressed using the law of large numbers (Gert and Enrique, 2008):

$$P\left\{\left|\hat{D}-\bar{D}\right|<\varepsilon_t\right\}=P\left\{\left|\frac{M}{\bar{A}_t}-\bar{D}\right|<\varepsilon_t\right\}>1-\alpha, \quad (4)$$

where $\hat{D}$ is the measured value of average defect density, $\bar{D}$ is the actual value of average defect density, $1-\alpha$ $(0<\alpha<1)$ is the confidence level, and ε_t is the estimation precision.

$\bar{A}_t$ can be cut into many small serpentine structures and these structures can be made exactly the same as each other. From Eq. (2), it can be inferred that if w and s remain the same, the average critical area of the obtained small serpentine structure will be directly proportional to $\bar{A}_t$. The $\bar{A}_t$ will be equal to the sum of the average critical areas of all these small serpentine structures. Because the small serpentine structures can be made small enough to have only one defect on them, the measured $\hat{D}$ could closely approach $\bar{D}$. According to the property of the Poisson distribution, each small serpentine test structure will obey the Poisson distribution and these small structures will be independent of each other. Assuming the mean and variance of the large serpentine structure is $\lambda_t=\bar{A}_t\bar{D}$, the mean and variance of each small serpentine structure will be $\bar{A}_s\bar{D}=\bar{A}_t\bar{D}/N_s=\lambda_t/N_s$.

As described in the Lindeberg-Levy theorem (Billingsley, 1961), if random variables $X_1, X_2, \ldots, X_n$ are independent of each other and they obey the same distribution with limited mathematical expectations and variances $E(X_i)=\mu$, $D(X_i)=\sigma^2\neq 0$ $(i=1, 2, \ldots, n)$, the following equation could be obtained:

$$\lim_{x\to\infty}P\left\{\frac{\sum_{k=1}^{n}X_k-n\mu}{\sqrt{n\sigma^2}}\leq x\right\}=\int_{-\infty}^{x}\frac{1}{\sqrt{2\pi}}\mathrm{e}^{-t^2/2}\mathrm{d}t=\Phi(x). \quad (5)$$

As described above, the divided small serpentine test structures are all independent of each other and they all obey the same Poisson distribution. Thus, with the use of the Lindeberg-Levy theorem described in Eq. (5), Eq. (4) can be rewritten as

$$P\left\{\left|\hat{D}-\bar{D}\right|<\varepsilon_t\right\}=2\Phi\left(\varepsilon_t\sqrt{\bar{A}_t/\bar{D}}\right)-1, \quad (6)$$

where the requirements for $\bar{A}_t$ have been changed to the form of the standard normal distribution. To satisfy the confidence level in Eq. (4), let $2\Phi\left(\varepsilon_t\sqrt{\bar{A}_t/\bar{D}}\right)-1>1-\alpha$, so requirements for $\bar{A}_t$ can be obtained as

$$\bar{A}_t>\frac{z_{\alpha/2}^2\bar{D}}{\varepsilon_t^2}, \quad (7)$$

where $z_{\alpha/2}$ is the upper fractile of the standard normal distribution. In Eq. (7), it is the total average critical area of all serpentine structures $\bar{A}_t$ that is obtained, but the total area of all serpentine structures A_{tc} in the actual chip may be preferred in practice. For a specific layout of serpentine test structure, the probability of failure θ is a constant. Using Eq. (3), the requirements for the total area of all serpentine structures A_{tc} can be derived:

$$A_{tc}>\frac{z_{\alpha/2}^2\bar{D}}{\varepsilon_t^2\theta}. \quad (8)$$

Just the satisfaction of the requirement in Eq. (8) is not enough to acquire a correct A_{tc}. Usually, to apply the Lindeberg-Levy theorem to the Poisson distribution correctly, the premise

$$\bar{A}_t\bar{D}=\theta A_{tc}\bar{D}\geq 20 \quad (9)$$

should be satisfied too. Considering Eqs. (8) and (9) simultaneously, the requirements for the total area of all serpentine structures A_{tc} can be summarized as

$$A_{tc}>z_{\alpha/2}^2\bar{D}/(\varepsilon_t^2\theta),\ \theta A_{tc}\bar{D}\geq 20. \quad (10)$$

As long as the inequalities above are satisfied, Eq. (4) will be satisfied. As a result, the actual value of average defect density $\bar{D}$ will be closely approached by

the measured average defect density $\hat{D}$, which will lie in the interval $(\bar{D}-\varepsilon_t, \bar{D}+\varepsilon_t)$ with a probability higher than $1-\alpha$.

3.2 Area of each serpentine test structure

In fact, the satisfaction of the requirement for the total area is not enough to acquire an accurate average defect density, because the area of each serpentine structure has an influence on the accuracy of this parameter too. Assuming the average critical area of a serpentine structure is $\bar{A}_s$, the yield of serpentine structures is $Y_s = e^{-\bar{A}_s\bar{D}}$. Taking the derivative of Y_s, the equation below can be obtained:

$$|\Delta Y_s| = \bar{A}_s e^{-\bar{A}_s\bar{D}} \Delta\bar{D}, \tag{11}$$

where ΔY_s is the change in Y_s and $\Delta\bar{D}$ is the change in $\bar{D}$. It can be inferred from Eq. (4) that the precision requirement for $\bar{D}$ is $\Delta\bar{D}=|\hat{D}-\bar{D}|<\varepsilon_t$. Substituting ε_t for $\Delta\bar{D}$, Eq. (11) can be rewritten as

$$\varepsilon_s = |\Delta Y_s| < \bar{A}_s e^{-\bar{A}_s\bar{D}} \varepsilon_t, \tag{12}$$

where ε_s is the estimation precision of the test structure yield. Eq. (12) shows the relation between the estimation precision ε_s of the test structure yield and the estimation precision ε_t of the measured average defect density.

For an accurate measurement of the yield of serpentine structures Y_s, the following equation should be met:

$$P\{|\hat{Y}_s - Y_s| < \varepsilon_s\} = P\left\{\left|\frac{H_s}{N_s} - Y_s\right| < \varepsilon_s\right\} > 1-\beta, \tag{13}$$

where $\hat{Y}_s$ is the measured yield of serpentine structures, Y_s is the actual yield of serpentine structures, and $1-\beta$ ($0<\beta<1$) is the confidence level for the yield of serpentine structures. Every tested result of each serpentine structure can be viewed as the result of a Bernoulli trial and these results are independent of each other. In the total N_s serpentine test structures, the number of opened serpentine structures H_s obeys the binominal distribution, which can be denoted as

$$P(H_s = k) = C_{N_s}^k Y_s^k (1-Y_s)^{N_s-k},\ k = 0, 1, 2, ... \tag{14}$$

As described in the DeMovire-Laplace theorem (Konno, 2002; Luo *et al.*, 2012), if random variable η_n obeys a binominal distribution with parameters of sample size n and probability p, for any x, it obeys

$$\lim_{x\to\infty} P\left\{\frac{\eta_n - np}{\sqrt{np(1-p)}} \le x\right\} = \int_{-\infty}^{x} \frac{1}{\sqrt{2p}} e^{-t^2/2} dt = \Phi(x). \tag{15}$$

When the premise of the normal distribution approximation

$$N_s Y_s = \frac{\bar{A}_t}{\bar{A}_s} e^{-\bar{A}_s\bar{D}} > 5 \tag{16}$$

is satisfied, the DeMovire-Laplace theorem in Eq. (15) can be applied to Eq. (13), and the following equation can be obtained:

$$P\{|\hat{Y}_s - Y_s| < \varepsilon_s\} \approx 2\Phi\left(\frac{N_s\varepsilon_s}{\sqrt{N_s Y_s(1-Y_s)}}\right) - 1. \tag{17}$$

As shown in Eq. (17), the requirement for the yield of serpentine structures Y_s has been changed to the form of a standard normal distribution. So as to satisfy the confidence level in Eq. (13), let

$$2\Phi\frac{N_s\varepsilon_s}{\sqrt{N_s Y_s(1-Y_s)}} - 1 > 1-\alpha,$$

and the requirement for the number of serpentine test structures N_s can be acquired:

$$N_s > \frac{z_{\beta/2}^2 Y_s(1-Y_s)}{\varepsilon_s^2}. \tag{18}$$

N_s can also be expressed in the form of the total average critical area of all serpentine structures $\bar{A}_t$ and the average critical area of a serpentine structure $\bar{A}_s$,

$N_s = \bar{A}_t/\bar{A}_s$. Substitute N_s with $\bar{A}_t/\bar{A}_s$, and substitute Y_s with the basic yield formula $Y_s = e^{-\bar{A}_s\bar{D}}$, and Eq. (18) can be rewritten as

$$\frac{\bar{A}_t\varepsilon_t^2}{z_{\beta/2}^2} > \frac{1-e^{-\bar{A}_s\bar{D}}}{\bar{A}_s e^{-\bar{A}_s\bar{D}}}. \tag{19}$$

Considering the premise of the normal distribution approximation in Eq. (16) and the requirement for the average critical area of a serpentine structure in Eq. (19) simultaneously, the requirements for the average critical area of each serpentine structure can be obtained as

$$\begin{cases} \dfrac{\bar{A}_t}{\bar{A}_s} e^{-\bar{A}_s\bar{D}} > 5, \\ \dfrac{\bar{A}_t\varepsilon_t^2}{z_{\beta/2}^2} > \dfrac{1-e^{-\bar{A}_s\bar{D}}}{\bar{A}_s e^{-\bar{A}_s\bar{D}}}. \end{cases} \tag{20}$$

In Eq. (20), note that it is the average critical area of each serpentine structure $\bar{A}_s$ that is obtained. In practice, the area of each serpentine structure A_{sc} in the actual chip may be preferred. If the area in Eq. (20) is denoted in the form of chip area, then by the use of Eq. (3), the requirements for the area of each serpentine structure can be acquired:

$$\begin{cases} \dfrac{A_{tc}}{A_{sc}} e^{-\theta A_{sc}\bar{D}} > 5, \\ \dfrac{\theta A_{tc}\varepsilon_t^2}{z_{\beta/2}^2} > \dfrac{1-e^{-\theta A_{sc}\bar{D}}}{\theta A_{sc} e^{-\theta A_{sc}\bar{D}}}. \end{cases} \tag{21}$$

Note that A_{tc} in Eq. (21) must satisfy the requirements in Eq. (10). Solve the set of inequalities and the upper limit of A_{sc} (that is, the upper limit of the area of each serpentine test structure) can be obtained. Unfortunately, explicit solutions cannot be acquired from the inequalities above, but numerical solutions can still be obtained by numerical calculation software.

3.3 Determination of optimal $\bar{A}_t$ and $\bar{A}_s$

After range requirements for the total area of serpentine test structures and the area of each serpentine structure are obtained, the measured average defect density of open defects on metal lines will be accurate enough and it could be used to predict metal yield for products. However, for different combinations of $\bar{A}_t$ and $\bar{A}_s$, the area occupied by the serpentine test structures differs significantly. To avoid wasting wafer by an inappropriate combination of $\bar{A}_t$ and $\bar{A}_s$, further investigation of optimal combination is needed.

For Eq. (7), $z_{\alpha/2}^2\bar{D}/\varepsilon_t^2$ can be denoted as $\bar{A}_b$, so $\bar{A}_t$ can be expressed as $K_b\bar{A}_b$ or $K_b z_{\alpha/2}^2\bar{D}/\varepsilon_t^2$, where K_b is a coefficient larger than 1. Then, Eq. (19) can be rewritten as

$$\frac{K_b z_{\alpha/2}^2\bar{D}}{z_{\beta/2}^2} > \frac{1-e^{-\bar{A}_s\bar{D}}}{\bar{A}_s e^{-\bar{A}_s\bar{D}}}. \tag{22}$$

If α and β take the same value, Eq. (22) can be further simplified as

$$K_b\bar{D} > \frac{1-e^{-\bar{A}_s\bar{D}}}{\bar{A}_s e^{-\bar{A}_s\bar{D}}}. \tag{23}$$

In actual test chips, serpentine structures are connected by pads, which are arranged in the form of a pad frame. Each serpentine line on a test structure has two pins, and thus a couple of pads are needed to test a serpentine test structure. The total area A_{total} occupied by the serpentine test structures including pads can be expressed as

$$A_{total} = 2A_{pad}N_s + A_{tc} = K_b\bar{A}_b\left(\frac{2A_{pad}}{\bar{A}_s} + \frac{1}{\theta}\right), \tag{24}$$

where A_{tc} is the total area occupied by the serpentine test structures without pads, and A_{pad} is the area that a pad occupies. Solve Eq. (23), which is the inequality determining the upper critical area limit of each serpentine test structure (IDUCALESTS), and then numerical solutions to $\bar{A}_s$ corresponding to each K_b can be acquired. Substitute these numerical solutions into Eq. (24), and then a series of different values of A_{total} can be obtained. Search the minimum area among these values and denote it as A_{total_min}, and then the values of K_b and $\bar{A}_s$ corresponding to A_{total_min} are just

the optimal K_{b_opt} and $\overline{A}_{s_opt}$. The optimal total average critical area of serpentine test structures can be calculated by $K_{b_opt}\overline{A}_b$.

The determination of optimal $\overline{A}_t$ and $\overline{A}_s$ in this paper is based on the area optimization. If the greatest concern is test time optimization instead of area optimization, the optimal choice of $\overline{A}_t$ and $\overline{A}_s$ will be different. The total testing time T_{total} for all serpentine structures can be expressed as

$$T_{total} = T_s N_s = \frac{\overline{A}_b T_s K_b}{\overline{A}_s}, \tag{25}$$

where T_s is the time used to test a serpentine structure. The solution process of optimal $\overline{A}_t$ and $\overline{A}_s$ for testing time optimization is similar to that for the minimum area optimization. Substitute numerical solutions to $\overline{A}_s$ corresponding to each K_b into Eq. (25), and then a series of T_{total} can be obtained. Search the minimum time among these values and denote it as T_{total_min}, and the values of K_b and $\overline{A}_s$ corresponding to T_{total_min} are just the optimal K_{bT_opt} and $\overline{A}_{sT_opt}$. For a specific confidence level and estimation precision, $\overline{A}_b$ is a constant; meanwhile, for a specific testing machine, T_s is also a constant, so the solution to minimum T_{total} is reduced to the solution to minimum $K_b/\overline{A}_s$. Eq. (24) can be modified to

$$A_{total} = 2\overline{A}_b A_{pad} \frac{K_b}{\overline{A}_s}\left(1 + \frac{\overline{A}_s}{2\theta A_{pad}}\right), \tag{26}$$

and the solution to minimum A_{total} can be reduced to the solution to minimum $(K_b/\overline{A}_s)\left(1+\overline{A}_s/(2\theta A_{pad})\right)$. $2A_{pad}$ can be viewed as a constant, but the value of $\overline{A}_s$ usually is comparable to the value of $2\theta A_{pad}$, so the latter item $\overline{A}_s/(2\theta A_{pad})$ in the brackets makes the optimal K_{bT_opt} and $\overline{A}_{sT_opt}$ quite different from the optimal K_{b_opt} and $\overline{A}_{s_opt}$. If testing time optimization is more important in a specific design of serpentine test structures, another combination of optimal $\overline{A}_t$ and $\overline{A}_s$ can be acquired from Eq. (26).

4 Simulations

Monte Carlo simulations are performed on computers with MatLab R2010b to verify the practical effect of the method proposed above. In the beginning, only the total area of serpentine test structures or only the area of each serpentine test structure is considered. In the latter part of simulations, both the total area of all serpentine test structures and the area of each serpentine test structure are considered. To facilitate comparison, the actual average defect densities used in the simulations are all 5 defects/mm^2.

Six groups of simulations considering the total average critical area $\overline{A}_t$ of all serpentine test structures are shown in Fig. 2 to illustrate the practical effect of Eq. (7). Defects data in each group are reproduced 10000 times. It is clearly shown that the deviation of the measured $\overline{D}$ will become more and more significant with the decrease of $\overline{A}_t$. Generally, in statistics, α is taken as 0.05 and thus the confidence level $1-\alpha$ is 0.95. Of course, if any other confidence level is required, the value of α can be taken according to actual demands. Compared with α, the estimation precision ε_t plays a more important role in determination of $\overline{A}_t$. The range of ε_t recommended is between the same order of magnitude as $\overline{D}$ and two orders of magnitude smaller than $\overline{D}$. For instance, if $\overline{D}$ =5 defects/mm^2, ε_t=1 defect/mm^2, and α=0.05, then the result of $\overline{A}_t$ calculated by Eq. (7) will be larger than 19.2 mm^2. The calculated result is in accordance with Fig. 2 rather well. For $\overline{A}_t$ larger than 19.2 mm^2, such as 500, 100, and 50 mm^2, more than 95% of the measured $\overline{D}$ are within 20% deviation. In contrast, for $\overline{A}_t$ smaller than 19.2 mm^2, such as 10, 5, and 1 mm^2, the proportion of the measured $\overline{D}$ within 20% deviation is less than 95%.

Another six groups of simulations only considering the average critical area of each serpentine test structure are shown in Fig. 3 to illustrate the

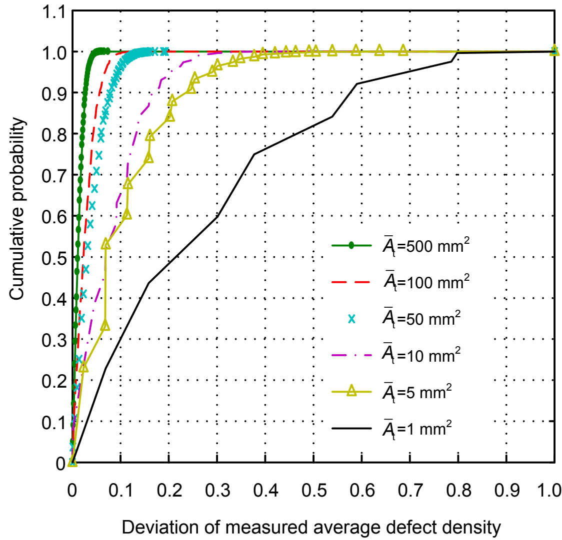

Fig. 2 Cumulative probability versus deviation of measured $\bar{D}$ ($\bar{A}_s$ is the same)

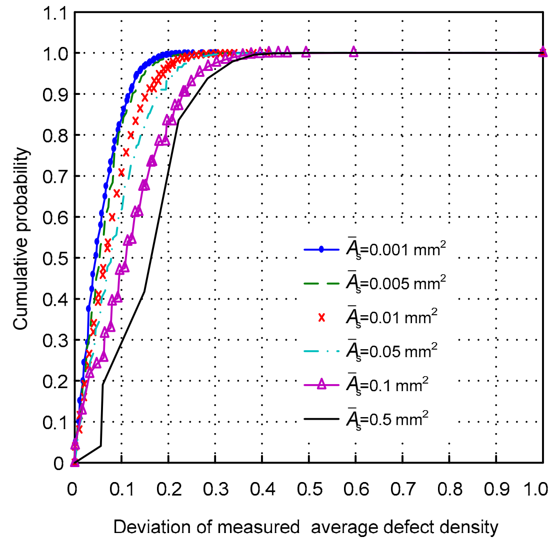

Fig. 3 Cumulative probability versus deviation of measured $\bar{D}$ ($\bar{A}_t$ is the same)

effect of Eq. (20). The total critical area A_t for six groups is all 1920.8 mm^2, which satisfies the requirement of A_t when α=0.05 and ε_t=1 defect/mm^2. Defects data in each group are reproduced 10 000 times. For comparison, the same defects data are tested six times as the data source of different groups, so the randomness of defects data for different groups is minimized. It is clearly shown that as A_s increases, the deviation of $\bar{D}$ becomes larger. The upper limit of the average critical area in each serpentine structure can be determined by Eq. (20). The values of β and ε_t can be taken in the same way as α and ε_t which have been discussed before. When A_t=1920.8 mm^2, β=0.05, and ε_t=1 defect/mm^2, the calculated upper limit of $\bar{A}_s$ is 0.0375 mm^2, which is in accordance with Fig. 3 quite well.

When both $\bar{A}_t$ and $\bar{A}_s$ are considered, the IDUCALESTS are derived. For precision consideration, the value of ε_t used in the next sets of simulations is taken as 0.1 defect/mm^2, which is one order of magnitude smaller than $\bar{D}$. The calculated results of $\bar{A}_s$ corresponding to different values of K_b are shown in Fig. 4, which is also the solution to IDUCALESTS. It can be seen that when K_b is small, the upper limit of $\bar{A}_s$ increases rapidly; while K_b is large, the rate of increase of the upper limit of $\bar{A}_s$ decreases.

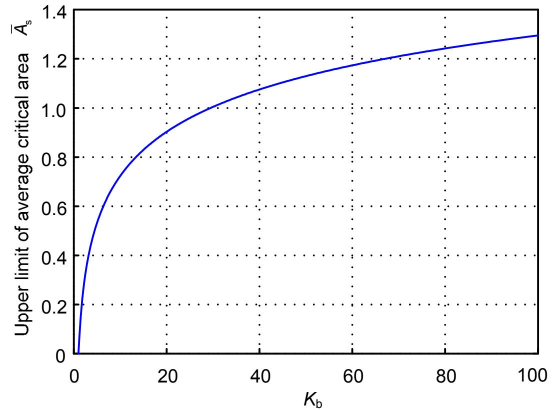

Fig. 4 Upper limit of $\bar{A}_s$ for inequality determining upper critical area limit of each serpentine test structure (IDUCALESTS)

Five groups of simulations are performed to further verify the consistency between simulations and IDUCALESTS when both $\bar{A}_t$ and $\bar{A}_s$ are considered. The results of these simulations are shown in Table 1. To minimize the differences between other experimental conditions, all groups in the table have the same theoretical $\bar{D}$ =5 defects/mm^2, ε_t=0.1 defect/mm^2, α=0.05, β=0.05, and number of tests 10 000. Different choices of K_b in each group result in different values of $\bar{A}_t$ and different upper limits of $\bar{A}_s$. In Groups 1, 3, 4, and 5, the percentages of tests with

deviations within ε_t are larger than 95%, which have reached our targeted confidence level. Group 2 is a reference group relative to Group 1, and the $\bar{A}_s$ in Group 2 is slightly larger than the calculated upper limit of $\bar{A}_s$ in IDUCALESTS. Correspondingly, the percentage of tests with deviations within ε_t does not meet the requirement of the confidence level $1-\alpha$, so the precision of IDUCALESTS is pretty good.

Table 1 Verification of the consistency between simulations and IDUCALESTS

Group	K_b	$\bar{A}_t$ (mm^2)	Upper limit of $\bar{A}_s$ (mm^2)	$\bar{A}_s$ (mm^2)	Deviation within ε_t (%)
1	1.05	2016.8	0.019 360	0.0193	95.04
2	1.05	2016.8	0.019 360	0.0194	94.95
3	5	9604.0	0.5321	0.53	95.02
4	25	48 020	0.9589	0.95	95.03
5	50	96 040	1.1293	1.12	95.01

IDUCALESTS: inequality determining upper critical area limit of each serpentine test structure

To find the optimal combination of $\bar{A}_t$ and $\bar{A}_s$ for area optimization, Eq. (24) is used to determine the two parameters. When $\bar{D}$ =5 defects/mm^2, ε_t=0.1 defect/mm^2, α=0.05, and β=0.05, the calculated $\bar{A}_b$ is 1920.8 mm^2. In SMIC 45 nm technology, the relation of A_{total} and K_b is as shown in Fig. 5. When K_b=1.10 and $\bar{A}_s$ =0.0375 mm^2, the minimum A_{total} acquired is 13 961 mm^2.

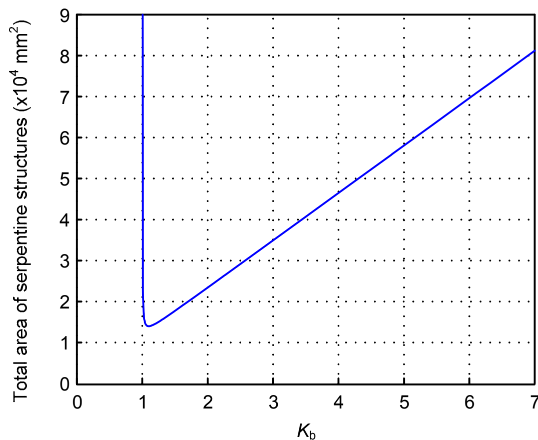

Fig. 5 Relation of A_{total} and K_b

5 Wafer experiments

Two types of serpentine test structures are designed and performed on test chips by SMIC 45 nm in our experiments. One type is a new serpentine test structure (NSTS) which is designed using the method proposed in this paper; the other type is the original serpentine test structure (OSTS) designed by previous design method. As conductive lines are denser in Metal-1, defects in this layer are easier to generate a faulty circuit, so the NSTS and OSTS are fabricated on Metal-1. To reduce the differences in the number of metal open defects caused by randomness, the NSTS and OSTS are designed on the same 350 test chips and the locations of the two types of test structures are designed close to each other on each test chip. The area of each test chip is 1 cm^2 and each test chip also includes other types of test structures. The NSTS and OSTS occupy only a small part of an entire test chip.

In OSTS, each serpentine structure occupies 0.118 mm^2 and each test chip has 32 serpentine structures, so the area occupied by OSTS on each test chip is 3.8 mm^2. The number of OSTSs is 11 200, so in total, there are 1321 mm^2 used in the fabrication of the OSTS. The area of each serpentine test structure and the total area of all serpentine test structures here are determined by previous experience of designers.

In NSTS, the optimal coefficient K_b calculated by Eq. (24) for area optimization is 1.07 when the confidence level and estimation precision are taken as 0.95 and 0.10 defect/mm^2, respectively. Correspondingly, the calculated minimal A_{total} is 7174 mm^2. The area of each serpentine test structure used here is 0.320 mm^2 and each test chip has 64 serpentine structures, so the area occupied by NSTS on each test chip is 20.5 mm^2.

The layout of an NSTS fabricated on the Metal-1 layer is shown in the lower part of Fig. 6. An NSTS is composed of two pads and many connected parallel metal lines. These metal lines occupy a region with length L and width H, and these two parameters are useful in critical area calculation using Eq. (2). The two pads, pad_A and pad_B, are boxed by dotted lines in the lower right of Fig. 6. The rest of the pads shown are used to measure test structures on other layers. A small part of NSTS is magnified in the upper part of Fig. 6 to show some details about the NSTS

layout. Two parameters w and s of metal lines are also labeled in Fig. 6, where w is the width of metal lines and s is the space between adjacent metal lines.

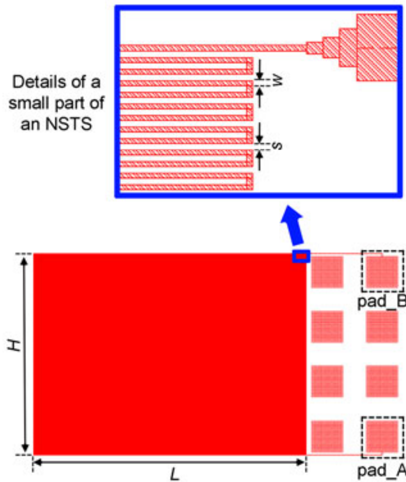

Fig. 6 Layout of a new serpentine test structure (NSTS)

An electrical test is needed to judge whether the serpentine test structure is open or not. When being tested, pad_A and pad_B of an NSTS are connected to two probe pins of a digital tester. A fixed voltage is applied to these two pads, and the generated current is monitored. Using Ohm's law, the resistance of an NSTS can be obtained by V/I, where V is the measured voltage and I is the measured current. The size of each NSTS is already known and the sheet resistance of Metal-1 is also known, so the theoretical resistance of an NSTS is acquired. To determine whether an NSTS is open or not, a threshold resistance R_{th} is set at least one order of magnitude larger than the theoretical resistance of an NSTS. When the measured resistance of an NSTS is smaller than R_{th}, the NSTS is thought to have no open faults; when the measured resistance of an NSTS is larger than R_{th}, the NSTS is believed to have open faults.

To fully investigate the measured results of the two types of serpentine test structures, 16 groups of experiments fabricated on test chips are performed. 350 test chips are contained in each group and the total number of test chips in all groups is 5600. In each group, an average defect density obtained by OSTS and an average defect density obtained by NSTS are acquired. Therefore, 32 measured average defect densities are obtained in total. The tested results are shown in Table 2.

Table 2 Measured results of 16 groups of wafer experiments

Group	N_{open}		Y_s		$\bar{D}$ (mm^2)	
	OSTS	NSTS	OSTS	NSTS	OSTS	NSTS
1	476	2807	0.9575	0.8746	2.7400	2.7004
2	479	2851	0.9572	0.8727	2.7577	2.7457
3	453	2770	0.9596	0.8763	2.6049	2.6623
4	459	2785	0.9590	0.8756	2.6401	2.6778
5	491	2864	0.9562	0.8721	2.8283	2.7592
6	464	2845	0.9586	0.8729	2.6695	2.7396
7	475	2823	0.9576	0.8739	2.7342	2.7169
8	457	2774	0.9592	0.8761	2.6284	2.6665
9	471	2804	0.9579	0.8748	2.7106	2.6973
10	458	2779	0.9591	0.8759	2.6342	2.6716
11	481	2857	0.9571	0.8724	2.7695	2.7519
12	463	2817	0.9587	0.8742	2.6636	2.7107
13	462	2796	0.9587	0.8751	2.6577	2.6891
14	503	2805	0.9551	0.8747	2.8991	2.6983
15	492	2907	0.9560	0.8702	2.8342	2.8036
16	481	2797	0.9571	0.8751	2.7695	2.6901

N_{open}: number of measured open serpentine test structures; Y_s: yield of serpentine test structures for OSTS and NSTS; $\bar{D}$: measured average defect density for OSTS and NSTS. NSTS: new serpentine test structure; OSTS: original serpentine test structure

Hypothesis testing is utilized to investigate the statistical significance of measured results of the two structures. More specifically, an F-test is used to evaluate whether the measured average defect densities have the same variance (Montgomery and Runger, 2002). If the null hypothesis H_{01} is $\sigma_1^2=\sigma_2^2$, and the alternative hypothesis is $\sigma_1^2\neq\sigma_2^2$, then the F statistic can be defined by

$$F=S_1^2/S_2^2, \tag{27}$$

where S_1^2 and S_2^2 are sample variances of the two types of serpentine test structures. The numbers of observations of OSTS and NSTS are both 16, so the degrees of freedom for the two structures are both 15. The significance level is set as 0.05 and the results of F-test are shown in Table 3. It is indicated from the values of the F statistic and two-tail P-value that variances of the two structures are significantly different. In addition, the variance of the NSTS is much smaller than the variance of OSTS, which means that

the measured average defect density of NSTS is more stable than that of OSTS.

Welch (1947)'s t test is used to further evaluate the statistical significance of the measured means of the two serpentine test structures. If the null hypothesis H_{02} is $\mu_1=\mu_2$, and the alternative hypothesis is $\mu_1\neq\mu_2$, then the t statistic can be expressed as

$$t=\frac{\overline{X}_1-\overline{X}_2}{\sqrt{\frac{S_1^2}{n_1}+\frac{S_2^2}{n_2}}},\qquad(28)$$

where $\overline{X}_1$ and $\overline{X}_2$ are sample means of the two types of test structures, n_1 and n_2 are numbers of observations of OSTS and NSTS, respectively. The Welch-Satterthwaite equation

$$\upsilon=\frac{\left(S_1^2/n_1+S_2^2/n_2\right)^2}{\frac{S_1^2/n_1}{n_1-1}+\frac{S_2^2/n_2}{n_2-1}}\qquad(29)$$

is used to approximate the degree of freedom associated with Welch's t test. When υ is not an integer, it will be rounded to calculate two-tail probabilities. The results of the t-test for the two serpentine test structures are shown in Table 4, where the significance level is taken as 0.05. Because the two types of test structures are fabricated on the same test chip and their locations are close to each other, the means of the OSTS and NSTS should not be significantly different. As shown in Table 4, this is also consistent with the results indicated by the t statistic and two-tail P-value.

It is revealed by the results of the two hypothesis tests that the means of the OSTS and NSTS are not significantly different while the variances of the two serpentine test structures are significantly different. By carefully designing the total area of all serpentine test structures and the area of each serpentine test structure, the NSTS has a more stable measured average defect density. In addition, the deviation between the measured and the actual average defect densities is believed to be within 0.1 defect/mm^2 with a probability higher than 95%. Hence, it is proved by various data that the NSTS designed using the proposed method has better performance.

6 Conclusions

With the increase of backend processes associated with metal layers, the confidence level and estimation precision of the measured average defect density become more important. The proposed method of determining the total area of all serpentine test structures and the area of each serpentine test structure changes the status of designing serpentine structures mainly based on past experience, and it increases the statistical significance of the measured average defect density, resulting in more convincing measured results. By carefully selecting actual requirements for confidence level and estimation precision, adequate combinations of the total area of all serpentine test structures and the area of each serpentine test structure can be acquired. Monte Carlo simulations show that the confidence level and estimation precision of the measured average defect density are indeed affected by the choices of the total

Table 3 Two-sample *F*-test for variances

Type	Mean	Variance	Number of observations	Degree of freedom	*F* statistic	Two-tail *P*-value	Two-tail *F* critical
OSTS	2.7213	0.007256	16	15	4.7296	0.0047	2.8600
NSTS	2.7113	0.001534	16	15			

Table 4 Two-sample Welch's *t*-test for means

Type	Mean	Variance	Number of observations	Degree of freedom	*t* statistic	Two-tail *P*-value	Two-tail *t* critical
OSTS	2.7213	0.007256	16	21	0.4279	0.6731	2.0796
NSTS	2.7113	0.001534	16	21			

area of all serpentine test structures and the area of each serpentine test structure. The results of other simulations are also consistent with the expected results of the proposed method. In wafer experiments, data collected from test chips fabricated by the SMIC 45 nm technology indicated that the proposed method has better performance. It should be noted that despite the focus on open failure of metal layer in this paper, the proposed designing method can be extended for other failure modes to extract more accurate parameters.

References

Arumi, D., Rodriguez-Montanes, R., Figueras, J., 2008. Experimental characterization of CMOS interconnect open defects. *IEEE Trans. CAD Integr. Circ. Syst.*, **27**(1): 123-136. [doi:10.1109/tcad.2007.907255]

Billingsley, P., 1961. The Lindeberg-Levy theorem for martingales. *Proc. Am. Math. Soc.*, **12**(5):788-792. [doi:10.2307/2034876]

Chen, F., Shinosky, M., Li, B., Aitken, J., Cohen, S., Bonilla, G., Simon, A., McLaughlin, P., Achanta, R., Baumann, F., *et al.*, 2011. Invasion Percolation Model for Abnormal TDDB Characteristic of ULK Dielectrics with Cu Interconnect at Advanced Technology Nodes. IEEE Int. Conf. on Reliability Physics Symp., p.2F.2.1-2F.2.8. [doi:10.1109/irps.2011.5784466]

Fayolle, M., Gayet, P., Morand, Y., 2000. Multilevel Test Structures for Metal CMP Integration Application to Cu/SiO_2 Damascene Interconnect. 3rd Annual Int. Interconnect Technology Conf., p.28-30. [doi:10.1109/iitc.2000.854271]

Gert, D.C., Enrique, M., 2008. Weak and strong laws of large numbers for coherent lower previsions. *J. Stat. Plan. Inf.*, **138**(8):2409-2432. [doi:10.1016/j.jspi.2007.10.020]

Hess, C., Saadat, M., Inani, A., Yun, L., Matsuhashi, H., Squicciarini, M., Lindley, R., Akiya, N., Kaste, E.F., 2006. Yield Improvement Using a Fast Product Wafer Level Monitoring System. IEEE/SEMI Advanced Semiconductor Manufacturing Conf. and Workshop, p.417-422. [doi:10.1109/ASMC.2006.1638794]

Hess, C., Inani, A., Joag, A., Sa, Z., Spinelli, M., Zaragoza, M., Long, N., Kumar, B., 2010. Stackable Short Flow Characterization Vehicle Test Chip to Reduce Test Chip Designs, Mask Cost and Engineering Wafers. IEEE/ SEMI Conf. on Advanced Semiconductor Manufacturing, p.328-333. [doi:10.1109/asmc.2010.5551474]

Hsu, C.L., Fang, J.Y., Yu, A., Lin, J., Huang, C., Wu, J.Y., Perng, D.C., 2009. Defect Study of Manufacturing Feasible Porous Low *k* Dielectrics Direct Polish for 45 nm Technology and Beyond. IEEE Int. Interconnect Technology Conf., p.140-142. [doi:10.1109/iitc.2009.5090365]

Jeong, T.Y., Choi, S.M., Baek, D.C., Windu, S., Lee, M., Park, J., 2012. Effective Line Length of Test Structure and OTS Effect of Area Scaling on TDDB Characterization in Advanced Cu/ULK Process. IEEE Int. Reliability Physics Symp., p.BD.3.1-BD.3.4. [doi:10.1109/irps.2012.6241877]

Karthikeyan, M., Medina, L., Shiling, E., Kiesling, D., 2010. 32 nm Yield Learning Using Efficient Parallel-Test Structures. IEEE/SEMI Advanced Semiconductor Manufacturing Conf., p.1-6. [doi:10.1109/asmc.2010.5551411]

Khare, J., Maly, W., Griep, S., Schmitt-Landsiedel, D., 1994. SRAM-Based Extraction of Defect Characteristics. Int. Conf. on Microelectronic Test Structures, p.98-107. [doi:10.1109/ICMTS.1994.303494]

Konno, N., 2002. Quantum random walks in one dimension. *Quantum Inf. Process.*, **1**(5):345-354. [doi:10.1023/a:1023413713008]

Kumar, M.V., Lukaszek, W., Plummer, J.D., 1997. A test structure advisor and a coupled, library-based test structure layout and testing environment. *IEEE Trans. Semiconduct. Manuf.*, **10**(3):370-383. [doi:10.1109/66.618210]

Lin, C.S., Huang, J.H., Hong, S.R., Lo, C.S., Chuang, L.S., 2002. Integration HDP CVD Oxide Sputtering Effect for Metal Void Defect Solution. Semiconductor Manufacturing Technology Workshop, p.165-168. [doi:10.1109/smtw.2002.1197400]

Lin, T.M.Z., Hsu, W.M., Lin, S.R., Wang, R.C.J., Chiu, C.C., Wu, K., 2006. Identification and Layout Modification of Copper/Low *k* Interconnect Dielectric Reliability Assessment by Using RVDB Test. 44th Annual IEEE Int. Reliability Physics Symp., p.687-688. [doi:10.1109/relphy.2006.251325]

Luo, X.H., Chen, L.S., Zhu, J.J., Yan, X.L., 2012. A new via chain design method considering confidence level and estimation precision. *J. Zhejiang Univ.-Sci. C (Comput. & Electron.)*, **13**(9):702-710. [doi:10.1631/jzus.C1200079]

Michalka, T.L., Lukaszek, W., Meindl, J.D., 1990. A redundant metal-polyimide thin film interconnection process for wafer scale dimensions. *IEEE Trans. Semic. Manuf.*, **3**(4):158-167. [doi:10.1109/66.61964]

Montgomery, D.C., Runger, G.C., 2002. Applied Statistics and Probability for Engineers (3rd Ed.). John Wiley & Sons, Inc., New York, p.356-359.

Roesch, W.J., Hamada, D.J.M., 2004. Studying Yield and Reliability Relationships for Metal Defects. Workshop on Reliability of Compound Semiconductors, p.121-133. [doi:10.1109/rocs.2004.184353]

Sayah, H.R., Buehler, M.G., 1988. Comb/Serpentine/ Cross-Bridge Test Structure for Fabrication Process Evaluation. IEEE Int. Conf. on Microelectronic Test Structures, p.23-28. [doi:10.1109/icmts.1988.672923]

Stapper, C.H., 1973. Defect density distribution for LSI yield calculations. *IEEE Trans. Electron Dev.*, **20**(7):655-657. [doi:10.1109/T-ED.1973.17719]

Stapper, C.H., 1983. Modeling of integrated circuit defect sensitivities. *IBM J. Res. Devel.*, **27**(6):549-557. [doi:10.1147/rd.276.0549]

Stapper, C.H., 1984. Modeling of defects in integrated circuit photolithographic patterns. *IBM J. Res. Devel.*, **28**(4): 461-475. [doi:10.1147/rd.284.0461]

Tamaki, Y., Ito, M., Takimoto, Y., Hashino, M., Kawamoto, Y., 2011. New Test Structure for Evaluating Low-*k* Dielectric Interconnect Layers by Using Ring-Oscillators and Metal Comb/Serpentine Patterns. 24th IEEE Int. Conf. on Microelectronic Test Structures, p.125-129. [doi:10.1109/icmts.2011.5976873]

Teh, W.H., Guo, L., Kumar, R., Kwong, D.L., 2005. 200-mm wafer-scale transfer of 0.18 μm dual-damascene Cu/SiO_2 interconnection system to plastic substrates. *IEEE Electron Dev. Lett.*, **26**(11):802-804. [doi:10.1109/led.2005.857734]

Wahab, Y.A., Ahmad, A.F., Awang, Z., 2006. Comparison of Missing Metal Defect Formation on He In-Situ and Furnace Annealed Electroplated Copper Films. 4th Student Conf. on Research and Development, p.53-57. [doi:10.1109/scored.2006.4339307]

Wallmark, J.T., 1960. Design considerations for integrated electronic devices. *Proc. IRE*, **48**(3):293-300. [doi:10.1109/JRPROC.1960.287597]

Welch, B.L., 1947. The generalization of ‘student’s’ problem when several different population variances are involved. *Biometrika*, **34**(1-2):28-35. [doi:10.2307/2332510]

Recommended paper related to this topic

A new via chain design method considering confidence level and estimation precision

Authors: Xiao-hua LUO, Li-sheng CHEN, Jiao-jiao ZHU, Xiao-lang YAN
doi:10.1631/jzus.C1200079
J. Zhejiang Univ.-Sci. C (Comput. & Electron.), 2012 Vol.13 No.9 P.702-710

Abstract: For accurate prediction of via yield, via chains are usually fabricated on test chips to investigate issues about vias. To minimize the randomness of experiments and make the testing results more convincing, the confidence level and estimation precision of the via failure rate are investigated in this paper. Based on the Poisson yield model, the method of determining an adequate number of total vias is obtained using the law of large numbers and the de Moivre-Laplace theorem. Moreover, for a specific confidence level and estimation precision, the method of determining a suitable via chain length is proposed. For area minimization, an optimal combination of total vias and via chain length is further determined. Monte Carlo simulation results show that the method is in good accordance with theoretical analyses. Results of via failure rates measured on test chips also reveal that via chains designed using the proposed method has a better performance. In addition, the proposed methodology can be extended to investigate statistical significance for other failure modes.